ADVANCES IN ATMOSPHERIC SCIENCES, VOL. 30, NO. 6, 2013, 1549–1559

Earth System Model FGOALS-s2: Coupling a Dynamic Global Vegetation and Terrestrial Carbon Model with the Physical Climate System Model

WANG Jun[1,2] (王 军), BAO Qing*[1] (包 庆), Ning ZENG[3], LIU Yimin[1] (刘屹岷), WU Guoxiong[1] (吴国雄), and JI Duoying[4] (纪多颖)

[1] *State Key Laboratory of Numerical Modeling for Atmospheric Sciences and Geophysical Fluid Dynamics, Institute of Atmospheric Physics, Chinese Academy of Sciences, Beijing* 100029

[2] *University of the Chinese Academy of Sciences, Beijing* 100049

[3] *Department of Atmospheric and Oceanic Science and Earth System Science Interdisciplinary Center, University of Maryland, College Park, Maryland, USA*

[4] *College of Global Change and Earth System Science, Beijing Normal University, Beijing* 100875

(Received 24 July 2012; revised 12 January 2013; accepted 16 January 2013)

ABSTRACT

Earth System Models (ESMs) are fundamental tools for understanding climate-carbon feedback. An ESM version of the Flexible Global Ocean–Atmosphere–Land System model (FGOALS) was recently developed within the IPCC AR5 Coupled Model Intercomparison Project Phase 5 (CMIP5) modeling framework, and we describe the development of this model through the coupling of a dynamic global vegetation and terrestrial carbon model with FGOALS-s2. The performance of the coupled model is evaluated as follows.

The simulated global total terrestrial gross primary production (GPP) is 124.4 PgC yr^{-1} and net primary production (NPP) is 50.9 PgC yr^{-1}. The entire terrestrial carbon pools contain about 2009.9 PgC, comprising 628.2 PgC and 1381.6 PgC in vegetation and soil pools, respectively. Spatially, in the tropics, the seasonal cycle of NPP and net ecosystem production (NEP) exhibits a dipole mode across the equator due to migration of the monsoon rainbelt, while the seasonal cycle is not so significant in Leaf Area Index (LAI). In the subtropics, especially in the East Asian monsoon region, the seasonal cycle is obvious due to changes in temperature and precipitation from boreal winter to summer. Vegetation productivity in the northern mid-high latitudes is too low, possibly due to low soil moisture there.

On the interannual timescale, the terrestrial ecosystem shows a strong response to ENSO. The model-simulated Niño3.4 index and total terrestrial NEP are both characterized by a broad spectral peak in the range of 2–7 years. Further analysis indicates their correlation coefficient reaches −0.7 when NEP lags the Niño3.4 index for about 1–2 months.

Key words: Earth System Model (ESM), Dynamic Global Vegetation Model (DGVM), carbon cycle, seasonal cycle, interannual variability

Citation: Wang, J., Q. Bao, N. Zeng, Y. M. Liu, G. X. Wu, and D. Y. Ji, 2013: Earth System Model FGOALS-s2: Coupling a dynamic global vegetation and terrestrial carbon model with the physical climate system model. *Adv. Atmos. Sci.*, **30**(6), 1549–1559, doi: 10.1007/s00376-013-2169-1.

1. Introduction

Anthropogenic CO_2 emissions from activities such as fossil fuel combustion may lead to major climate change in the coming century. However, the responses and feedback of terrestrial ecosystems and oceans to elevated atmospheric CO_2 concentrations and concomitant climatic changes remain highly uncertain

*Corresponding author: BAO Qing, baoqing@mail.iap.ac.cn

(Friedlingstein et al., 2006; Denman et al., 2007). To date, fully coupled carbon/climate models have proved to be useful tools in uncovering background scientific implications and providing valuable reference estimates of feedback strength. Therefore, looking ahead, the development of state-of-the-art Earth System Models (ESMs) has become a major goal for model development teams within the atmospheric science community.

The carbon cycle was first researched by means of *in situ* observations. Long-term observations of atmospheric CO_2 concentrations began in 1958 at Mauna Loa, Hawaii. However, with the emergence of dynamic vegetation models in the mid-1990s, such as land–atmosphere interaction model (AVIM; Ji, 1995), Integrated Biosphere Simulator (IBIS; Foley et al., 1996), Vegetation Continuous Description model (VECODE; Brovkin et al., 1997) and Top-down Representation of Interactive Foliage and Flora Including Dynamics (TRIFFID; Cox, 2001), scientists began to further research the feedback between the carbon cycle and climate change with fully coupled carbon/climate models that simultaneously included Dynamic Global Vegetation Models (DGVMs) and ocean biogeochemical processes. For instance, Cox et al. (2000) found that carbon cycle feedback could accelerate global warming, and although such positive feedback between the carbon cycle and global warming was frustrating, it was further confirmed by Dufresne et al. (2002) and Zeng et al. (2004) with their own earth system models. Friedlingstein et al. (2006) demonstrated that there was consensus among eleven models participating in the Coupled Carbon Cycle Climate Model Intercomparison Project (C^4MIP), that future climate change will weaken the ability of land and oceans to absorb anthropogenic CO_2. However, the magnitude of the positive feedback between the carbon cycle and climate remains largely uncertain with regard to the discrepancies among different models. In short, just as Heimann and Reichstein (2008) pointed out, current experiments have given us ambiguous results and have not provided us with definite conclusions.

At the State Key Laboratory of Numerical Modeling for Atmospheric Sciences and Geophysical Fluid Dynamics (LASG), Institute of Atmospheric Physics (IAP), a first generation air–sea coupled model, named the Global Ocean Atmosphere Land System (GOALS), was released at the end of the 20th century when it participated in the third IPCC Assessment Report (Zhang et al., 2000). In 2004, GOALS was updated to the Flexible Global Ocean–Atmosphere–Land System (FGOALS-s1) model, which was driven by a flux coupler (Bao et al., 2006), and was then followed by a modified version, FGOALS-s1.1 (Bao et al., 2010). However, none of these versions included any biogeochemical modules, and it is therefore urgent for the model community to develop an ESM version of FGOALS.

Considering the already reported strong performance of VEGAS (Vegetation–Global–Atmosphere–Soil), a dynamic global vegetation and terrestrial carbon model, in an ESM model (Zeng et al., 2004), we coupled version 2.0 of this model (VEGAS2.0) to FGOALS-s2 as a terrestrial ecosystem and carbon cycle component, to create an ESM version of FGOALS (hereafter ESM FGOALS-s2). VEGAS2.0 took the place of the Community Land Model's Dynamic Global Vegetation Model (CLM3.0-DGVM), which does not support fully coupled carbon simulations (Levis et al., 2004). In this context, we report results from an offline and coupled run of the coupled model as follows. Section 2 presents a description of the model, as well as the implementation of the coupling. Section 3 describes the datasets used and the experimental design. The performance of the DGVM in ESM FGOALS-s2 is discussed in section 4. And finally, we present further discussion and draw conclusions from the study in sections 5 and 6, respectively.

2. The models and their coupling process

The physical climate model used was the Flexible Global Ocean–Atmosphere–Land System, Spectral Version 2 (FGOALS-s2) (Bao et al., 2012), which comprises the Spectral Atmospheric Model of IAP LASG (SAMIL) and LASG IAP Common Ocean Model (LICOM). The sea-ice component of FGOALS-s2 is version 5 of the CCSM sea ice model (CSIM5) (Collins et al., 2006), the land component is CLM3.0 (Oleson et al., 2004), and the coupler used to drive the four major components is the sixth version of the National Center for Atmospheric Research (NCAR) flux coupler (Collins et al., 2006).

The dynamic global vegetation model used was the second version of VEGAS (VEGAS2.0; Zeng, 2003; Zeng et al., 2004, 2005). This model is able to simulate the spatial and temporal evolution of terrestrial vegetation and contains five plant functional types (PFTs): needleleaf trees, broadleaf trees, C3 grass, C4 grass, and crop. It also includes independent modules for land-use and fire. Considering the inconsistencies of the forms of the land-use datasets between VEGAS2.0 and CLM3.0, we switched off the land-use module and the crop PFT. We also turned off the fire module, but will include this in future work. Competition, the determination of the fractional cover among the different PFTs, is under the control of the climatic constraints and resource allocations within the model. The total

terrestrial carbon pools consist of vegetation and soil pools, with the former being further divided into leaf, sapwood, heartwood, coarse root, and fine root, while the latter consists of metabolic, structural, fast soil, medium soil, and slow soil pools.

To a large extent, the performance of VEGAS2.0 is determined by the climatic fields. It treats eight variables as the forcing fields: the surface soil layer temperature (Tsm, which is averaged from the first to the third layer in CLM3.0); the second soil layer temperature (Ts2m, which is averaged from the fourth to the tenth layer); bottom air temperature (Tairsm); soil relative moisture (Swetm); surface layer soil relative moisture (Swet1m); downward solar radiation (FSWdm); runoff (Runfm); and CO_2 concentration (CO2atmov), obtained from CLM3.0. The coupling frequency between VEGAS2.0 and CLM3.0 is one day. Considering the unmatched PFTs between VEGAS2.0 and CLM3.0, we placed VEGAS2.0 on the grid level of CLM3.0. VEGAS2.0 only feeds CO_2 flux back to the atmospheric model. In view of the mismatches between the simulated leaf area index (LAI) by VEGAS2.0 and satellite-based LAI used in CLM3.0, the LAI and stem area index (SAI), affecting the surface albedo's calculation on land, do not get returned to CLM3.0.

3. Reference datasets and experimental design

The observational datasets used to evaluate the model's results included air temperature, precipitation, LAI, and soil liquid water volumetric content. The air temperature and precipitation data were made from Climatic Research Unit (CRU) datasets (resolution: 2.5°×2.5°) (Mitchell and Jones, 2005). The LAI data were mainly from Boston University (Myneni et al., 1997) and Hagemann (2002), and owing to the different periods, we principally highlight the seasonal evolution of LAI. Finally, the data for soil liquid water volumetric content came from the Climate Forecast System Reanalysis Project (CFSR; Saha et al., 2010).

The spin-up processes included two stages (Table 1), enabling the fully coupled integration to quickly reach a state of equilibrium. Firstly, the offline VEGAS2.0 was driven by pre-industrial climatology (Taylor et al., 2009) from physical climate system model (PCSM) FGOALS-s2 in the coupled framework with the data models. In this stage, we were able to quickly achieve the growth of vegetation and accumulations of the carbon pools (Fig. 1). In the second stage, VEGAS2.0 was coupled with PCSM FGOALS-s2 to make a continued run such that all surface flux and state variables were able to have some appropriate adjustments. In total, it took more than 700 years for ESM FGOALS-s2 to reach a state of equilibrium. Performances of the equilibrium state of ESM FGOALS-s2 are presented below.

4. Results

4.1 *Climatology*

The time series of some main variables in VEGAS2.0 in the offline step from model years 1–500 are presented in Fig. 1. In this run, we turned on the accelerator (which can increase the time step for slow processes to quickly reach the equilibrium) for the soil carbon pools to make them reach equilibrium as fast as possible for the first 200 years. All the variables varied little for the last 300 years. In Figs. 1a and b, the global total terrestrial gross primary production (GPP) is 122.4 PgC yr^{-1} (Table 2), corresponding to the observation-based estimate of 123±8 PgC yr^{-1} provided by Beer et al. (2010). Autotrophic respiration (R_a) is 70.1 PgC yr^{-1}. According to the equation

$$\mathrm{NPP} = \mathrm{GPP} - R_a \,, \tag{1}$$

where NPP denotes net primary production, the simulated global total terrestrial NPP has a value of 52.3 PgC yr^{-1}, which lies within the range of 44.4–66.3 PgC yr^{-1} (Cramer et al., 1999). Considering heterotrophic respiration (R_h) is equivalent to 52.1 PgC yr^{-1}, the net ecosystem production (NEP) is near to zero, showing the model has reached equilibrium. Figure 1c indicates the processes of carbon accumulation in the vegetation and soil pools during the offline spinup. In summary, the total terrestrial carbon pools simulated in VEGAS2.0 store 2270.7 PgC, comprising 640.5 PgC in the vegetation pools and 1630.2 PgC in the soil (Table 2).

Table 1. Experimental design for the OFFLINE and COUPLED runs.

Experiment name	Forcing fields/boundary conditions	Active models
OFFLINE	Climatological daily forcing fields of PCSM FGOALS-s2 in the pre-industrial run	Land component of PCSM FGOALS-s2 and VEGAS2.0
COUPLED	Boundary conditions in the pre-industrial run (greenhouse gases, solar constant, aerosol, ozone)	PCSM FGOALS-s2 and VEGAS2.0

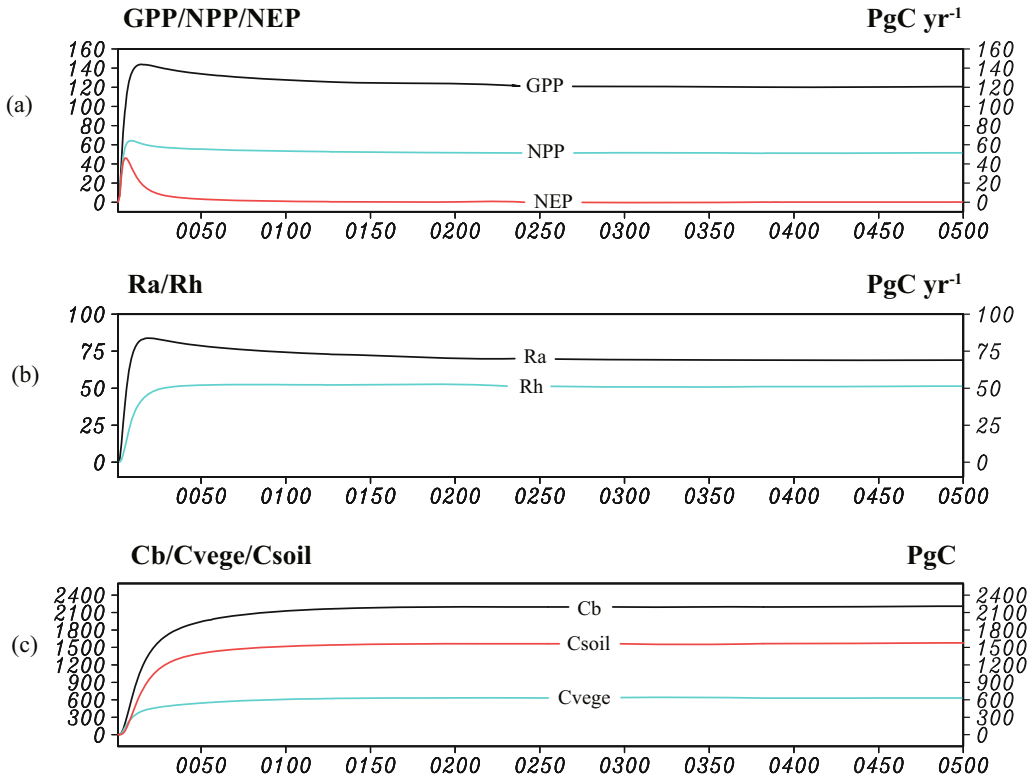

Fig. 1. Time-evolution of some main variables of VEGAS2.0 in the offline spin-up process from model years 1–500. The spin-up process was forced by the climatological states of the PCSM FGOALS-s2. "R_a" denotes autotrophic respiration, "R_h" denotes heterotrophic respiration, "C_b" denotes the total terrestrial carbon pool, "C_{vege}" denotes the vegetation carbon pool, and "C_{soil}" denotes the soil carbon pool.

Table 2. The global total terrestrial carbon fluxes and pools. In the offline run these are averaged from model years 471–500, while in the coupled run they are averaged from model years 1670–99.

	Global total terrestrial carbon fluxes and pools	
Variables (units)	OFFLINE	COUPLED
GPP (PgC yr^{-1})	122.4	124.4
R_a (PgC yr^{-1})	70.1	73.5
R_h (PgC yr^{-1})	52.1	50.9
C_b (PgC)	2270.7	2009.9
C_{soil} (PgC)	1630.2	1381.6
C_{vege} (PgC)	640.5	628.2

Compared to the offline results, the global total terrestrial carbon fluxes and pools averaged from model years 1670–1699 in ESM FGOALS-s2 are also listed in Table 2. Generally speaking, the states of equilibrium of VEGAS2.0 in ESM FGOALS-s2 are very similar to the offline states. The GPP is 124.4 PgC yr^{-1} and NPP (Rh) is 50.9 PgC yr^{-1}. The total terrestrial carbon pools contain 2009.9 PgC, with 628.8 PgC and 1381.6 PgC in the vegetation and soil pools, respectively. These results, both offline or in the coupled run, are close to the model-mean estimates by ten models participating in C4MIP (Qian et al., 2009).

Figure 2 shows the spatial distributions of GPP and total terrestrial carbon storage averaged from model years 1670–1699 in ESM FGOALS-s2. As shown in Fig. 2a, the spatial distribution of GPP is reasonable. GPP peaks in the tropics, characterized by rainforests and savannahs owing to plentiful rainfall and warm air temperatures all year round. The annual-averaged GPP is above 1.8 kg m^{-2} yr^{-1}. However, GPP in the northern mid-high latitudes is below 0.4 kg m^{-2} yr^{-1}, somewhat smaller than observation-based estimates (Beer et al., 2010). In desert regions, the carbon flux is non-zero because atmospheric model-simulated precipitation is non-zero there. The zonal mean of GPP indicates that GPP declines from the tropics to the high latitudes. Compared to observation-based estimates (Beer et al., 2010), GPP in the tropics and northern mid-high latitudes is a little weaker, whereas it is too strong in the subtropics, a region largely characterized by deserts.

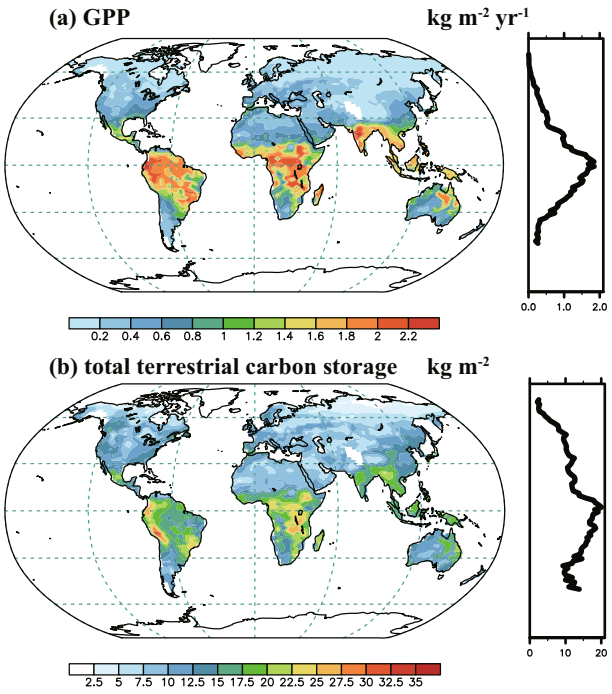

Fig. 2. Global distributions of the VEGAS-simulated GPP and total terrestrial carbon storage (vegetation + soil carbon) averaged from model years 1670–1699 in the fully coupled run. (a) GPP (units: kg m^{-2} yr^{-1}); (b) total terrestrial carbon pools (units: kg m^{-2}). The zonal mean curves are on the right-hand side of the figure.

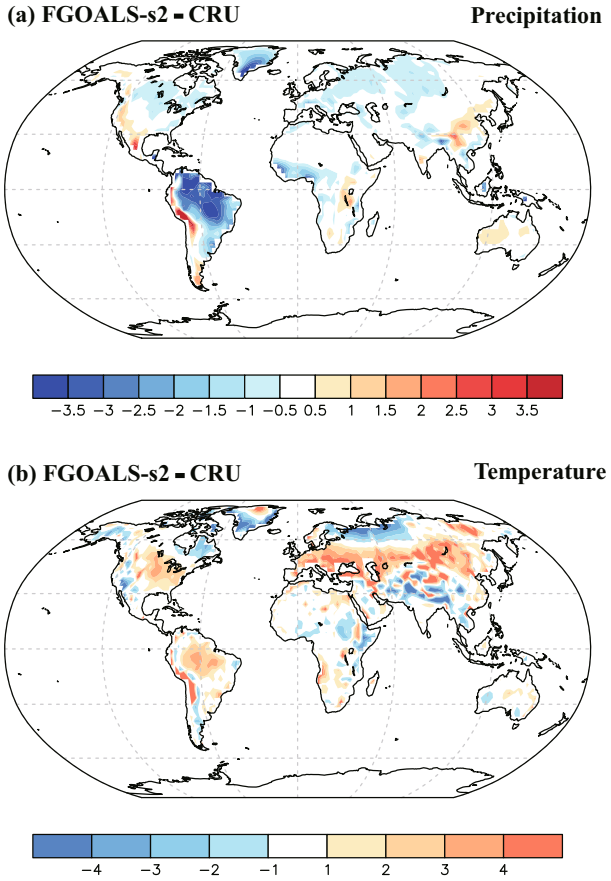

Fig. 3. Climatological differences of precipitation and air temperature between ESM FGOALS-s2 and CRU datasets for (a) precipitation deviation (units: mm d^{-1}) and (b) air temperature deviation (units: K).

In this respect, precipitation over land simulated by FGOALS-s2 could be further improved.

Figure 2b shows the distribution of total terrestrial carbon storage, including vegetation and soil organic carbon. The simulated spatial pattern is analogous to GPP, with the higher values distributed in the lower latitudes. However, in view of the low decomposition of soil organic carbon under low temperatures in nature, the soil carbon pool should have shown large amounts in the high latitudes, converted from the turnover of boreal forests. Furthermore, considering the soil carbon pool is about two or three times that of vegetation storage, there should have been another peak in the northern mid-high latitudes in the zonal-mean figure. Concerning the fact that soil organic carbon originates from the turnover of vegetation, this bias in the total terrestrial carbon storage simulated by ESM FGOALS-s2 is attributed to poorly simulated boreal forests in the high latitudes.

Figure 3 shows the climatological differences of precipitation and air temperature between ESM FGOALS-s2 and CRU datasets. Rainfall in the Amazon Basin shows a large bias (3 mm d^{-1} less than CRU), along with less rainfall ranging between −0.5 mm d^{-1} and −1.5 mm d^{-1} in the Sahel and western Eurasia, whereas more precipitation occurs in some desert regions such as the Australian Desert. Less rainfall results in less soil moisture, reducing the simulation of the growth and distribution of vegetation. Figure 3b shows that the temperature in ESM FGOALS-s2 is higher than CRU in the Amazon Basin and Northern Hemisphere mid-high latitudes. In the tropics, higher air temperature may stress the growth of vegetation, while it will contribute to growth in the mid-high latitudes. However, conversely, higher temperatures can accelerate the hydrological cycle through high levels of evaporation that will further decrease the soil moisture, creating adverse conditions for vegetation growth. Less precipitation and more evaporation conspire to inhibit needleleaf tree growth in the northern mid-high latitudes.

4.2 *Seasonal cycle*

The seasonal cycle of the terrestrial ecosystem is a basic characteristic of phenology dominated by the climate annual cycle. Figure 4 illustrates the differences of terrestrial GPP, NPP, and NEP between boreal summer (JJA) and boreal winter (DJF), as simu-

lated by ESM FGOALS-s2. In the tropics, excluding the desert regions, both NPP and NEP show an obvious dipole pattern with respect to the equator that resembles the distribution of precipitation (see below). The spatial pattern of GPP (Fig. 4a) is similar to that of NPP and NEP, though the amplitude is weaker. This phenomenon demonstrates that the migration of the monsoon rainbelt across the equator from boreal winter to boreal summer has the last word in the vegetation seasonal cycle in these regions. Yet, in the subtropics, especially in the East Asian monsoon region, vegetation flourishes (GPP/NPP/NEP increase) with the increase in rainfall after the break-up of the summer monsoon and warm temperatures in the summertime. In the northern mid-high latitudes, considering the weak change in the rainfall, temperature plays the most important role in the larger GPP, NPP, and NEP in JJA. Therefore, it is a fact that different climatic factors take control of the seasonal cycle of vegetation in different regions. According to

$$\mathrm{NEP} = \mathrm{NPP} - R_{\mathrm{h}} \,, \tag{2}$$

we can deduce that the seasonal cycle of R_{h} is analogous to the evolution of NPP (figure omitted). Warmer and wetter conditions in summertime generally contribute to the decomposition of the soil carbon pools.

LAI is another important variable in DGVMs that not only reflects the distributions of terrestrial vegetation, but also determines the albedo in vegetated regions. Figure 5 shows the distributions of LAI in JJA and DJF, and the difference between JJA and DJF for ESM FGOALS-s2, Boston University datasets, and Hagemann datasets. Obviously, discrepancies in magnitude exist in the two datasets, unmasking a fact that the reference data of the terrestrial ecosystem still remain largely uncertain. However, temporal evolution of the seasonal cycle in the two datasets is similar. In JJA, the LAI in the northern mid-high latitudes is about 4–6, whereas it is less than 2 in DJF, somewhat affected by snow cover. This demonstrates that LAI has a significant seasonal cycle to the north of the 45°N. Conversely, the seasonal cycle of LAI in the southern mid-high latitudes is not so remarkable (Figs. 5h and i). In ESM FGOALS-s2, the simulated LAI in the northern mid-high latitudes in JJA is less than 3, close to that in DJF (Figs. 5a and d). This indicates the seasonal cycle of simulated LAI in the northern mid-high latitudes in ESM FGOALS-s2 is not a good reflection of observed data, and can mainly be attributed to the poorly simulated boreal forests largely constrained by less precipitation (Fig. 3a). However, in the southern mid-high latitudes, the seasonal evolution is similar to the reference datasets (Fig. 5g). In

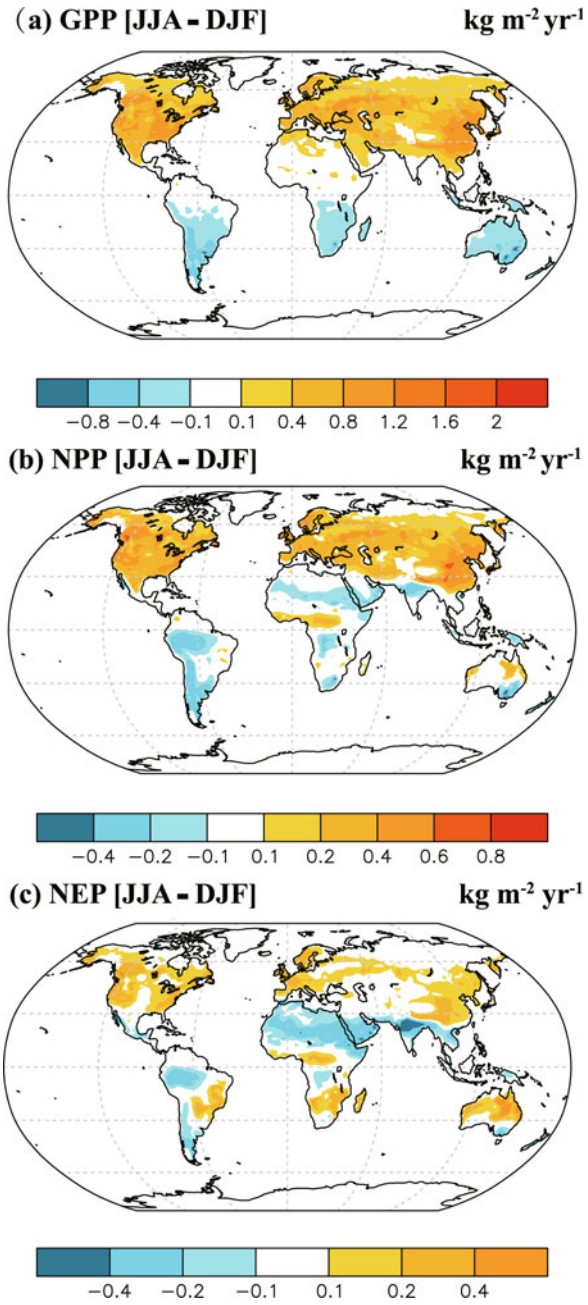

Fig. 4. The differences of VEGAS-simulated GPP, NPP and NEP between JJA and DJF for (a) GPP, (b) NPP and (c) NEP distributions in ESM FGOALS-s2 (units: kg m^{-2} yr^{-1}).

the subtropics, especially in the East Asian monsoon region, a pronounced seasonal evolution is a common feature (Figs. 5g–i) because of changes in precipitation and temperature from boreal winter to boreal summer. In the tropics, such as the rainforest region of the Amazon Basin, LAI does not show a significant seasonal cycle because of the warm and pluvial climate all year round (Figs. 5g–i), which is comparatively well simu-

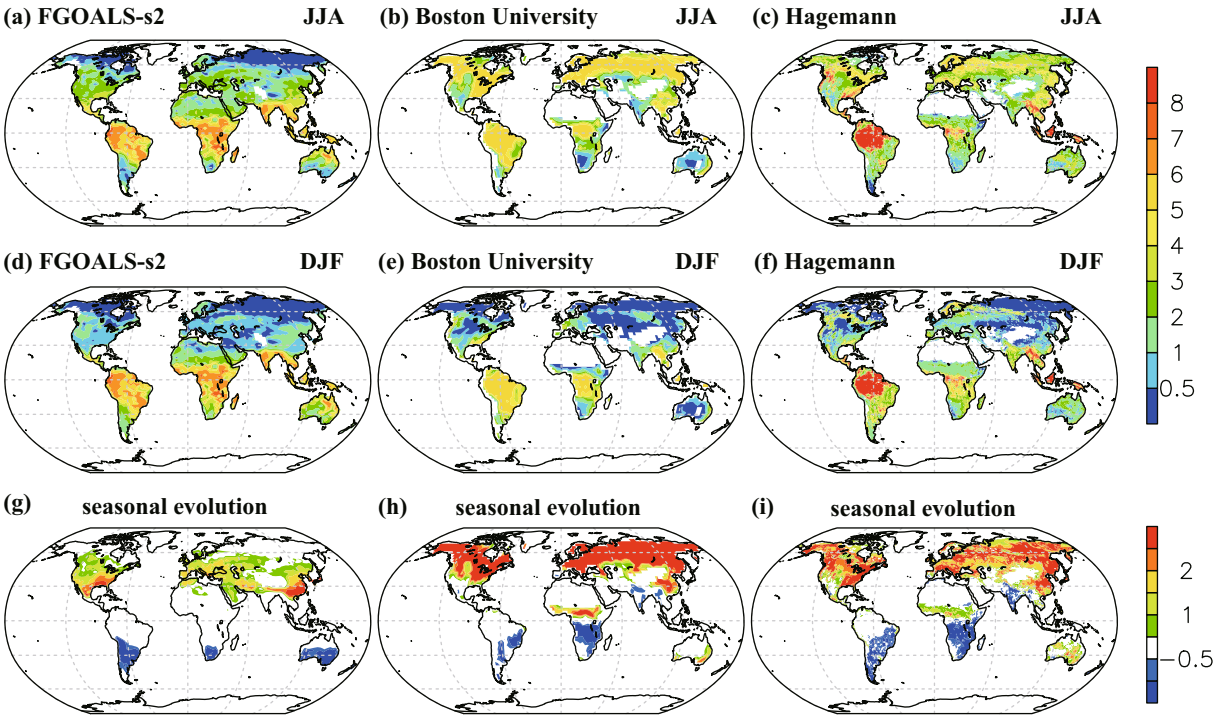

Fig. 5. Distributions of LAI (units: m^2 m^{-2}) in JJA and DJF, and differences between JJA and DJF for LAI simulated by ESM FGOALS-s2 (model years 1670–99) in column one, Boston University datasets (1982–2000) in column two, and Hagemann datasets (1982) in column three. Although the datasets cover different periods, they can still reflect the seasonal cycle of LAI.

lated by ESM FGOALS-s2 (Figs. 5a and d) relative to the reference datasets (Figs. 5b, c, e and f). Meanwhile, in the savannah regions of Africa, LAI in ESM FGOALS-s2 is slightly larger and does not show strong seasonal change, whereas there is noticeable seasonal change in the reference datasets because of the shift of the wet and dry season along with the migration of the monsoon rainbelt (Fig. 6c).

Figure 6 shows the differences of precipitation and temperature in ESM FGOALS-s2 and CRU between JJA and DJF. The seasonal evolution of precipitation (Figs. 6a and c) exhibits a dipole mode across the equator in response to the migration of the monsoon rainbelt in the tropics. However, the amplitude of precipitation in ESM FGOALS-s2 is slightly weaker, which has a large impact on the seasonal change of GPP, NPP, NEP and LAI in the tropics (Figs. 4 and 5). This bias partially explains the absence of a seasonal cycle of LAI in the African savannah, which is different from the observed patterns. Relatively, the seasonal change of air temperature (Figs. 6b and d) is simpler and more similar. The amplitude of air temperature change is small in the low latitudes and large in high latitudes. Air temperature changes simulated by ESM FGOALS-s2 are slightly larger compared to those seen in the CRU datasets for the northern mid-high latitudes. In spite of this, the seasonal cycle of LAI in the northern mid-high latitudes still shows large biases (Fig. 5g) because of the poorly simulated boreal forests. In short, both rainfall and air temperature take control of the seasonal cycle of the terrestrial ecosystem, though they may play different roles in different regions.

4.3 *Interannual variability*

Records of atmospheric CO_2 concentration at Mauna Loa since 1958, known as the Keeling Curve, indicate substantial interannual variability superimposed on a pronounced seasonal cycle and long-term trend (Keeling et al., 1976). Since then, the relationship between atmospheric CO_2 growth rate and El Nino-Southern Oscillation (ENSO) has been verified (Bacastow, 1976; Keeling and Revelle, 1985; Jones et al., 2001; Zeng et al., 2005; Qian et al., 2008). The terrestrial ecosystem, as one of the planet's carbon reservoirs, accounts for the interannual variability rather than the ocean (Bousquet et al., 2000; Jones et al., 2001), and thus the interannual variability is a crucial test for carbon cycle models.

Figure 7 shows the relationships between global total terrestrial NEP and the Niño3.4 sea surface

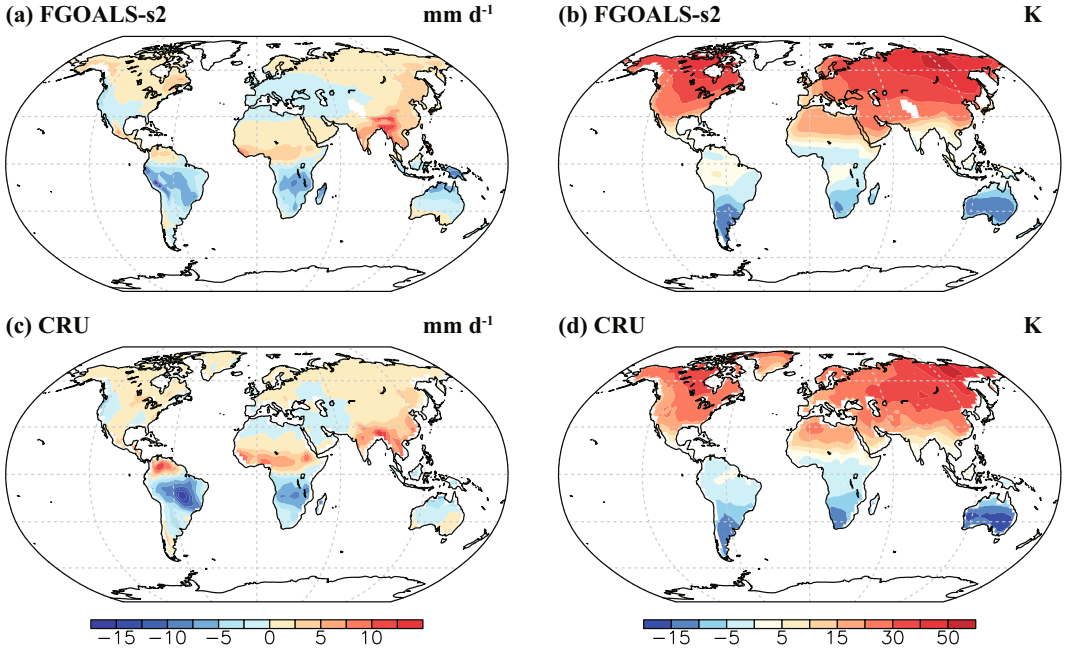

Fig. 6. The differences of precipitation and air temperature in ESM FGOALS-s2 and CRU datasets between JJA and DJF for (a, c) the difference of precipitation (units: mm d^{-1}) and (b, d) the difference of air temperature (units: K).

temperature anomaly (SSTA), as simulated by ESM FGOALS-s2. Figure 7a depicts the monthly time series of the Nino3.4 SSTA and global total terrestrial NEP (seasonal cycle removed). As can be seen, the amplitude of interannual variability of the Nino3.4 index is very reasonable. The time series of NEP also exhibits significant interannual fluctuations (ranging between ±3 PgC yr^{-1}) that is correlated with the Nino3.4 index. This phenomenon results from a "conspiracy" of the temperature, precipitation, and plant soil physiology (Zeng et al., 2005). However, variations between NEP and the Nino3.4 index are not perfectly in phase by comparison. Figure 7b shows the lead-lag correlation between them. It demonstrates that the negative correlation peaks with a value of −0.7 when the NEP lags the Nino3.4 index for approximately 1–2 months. This is principally caused by the memory property of the soil moisture. However, according to a study by Qian et al. (2008), based on observations, the interannual variability of the carbon flux between the land and atmosphere lags ENSO by about 5–6 months. This discrepancy is due to the weak capacity of soil water storage in the land component. Figures 7c and d show the power spectral analyses of the Niño3.4 index and global total terrestrial NEP, respectively. As can be seen, both of them show the significant 2-yr period. The NEP also shows the significant 4-yr period that is not so remarkable in the Niño3.4 index results. Further, an interesting phenomenon can be seen in that the strongest signal in NEP is the 4-yr period, in contrast to the 2-yr period for the Niño3.4 index. This inconsistency in period is largely determined by the soil filtering effect, which needs further research. In brief, the negative correlation between the Niño3.4 index and global total terrestrial NEP is noticeable in the fully coupled model.

5. Discussion

As mentioned above, the bias of precipitation in the model will influence the simulation of the growth and distribution of vegetation. However, photosynthesis is entirely under the control of air temperature, soil relative moisture, downward solar radiation, and CO_2 concentration in the atmosphere in VEGAS2.0. So, precipitation does not directly influence the carbon assimilation process, but is an important surface source for soil water. In CLM3.0, soil water is also affected by evaporation, surface and sub-surface runoff, gradient diffusion, infiltration, root extraction, and so on (Oleson et al., 2004) (in the present study, runoff in FGOALS-s2 was switched off). In other words, soil moisture is simultaneously affected by precipitation simulated by the atmospheric component and the parameterizations of the associated processes upon the hydrological cycle in CLM3.0.

Figure 8 shows the distributions of liquid water volumetric content in the land model of ESM FGOALS-s2

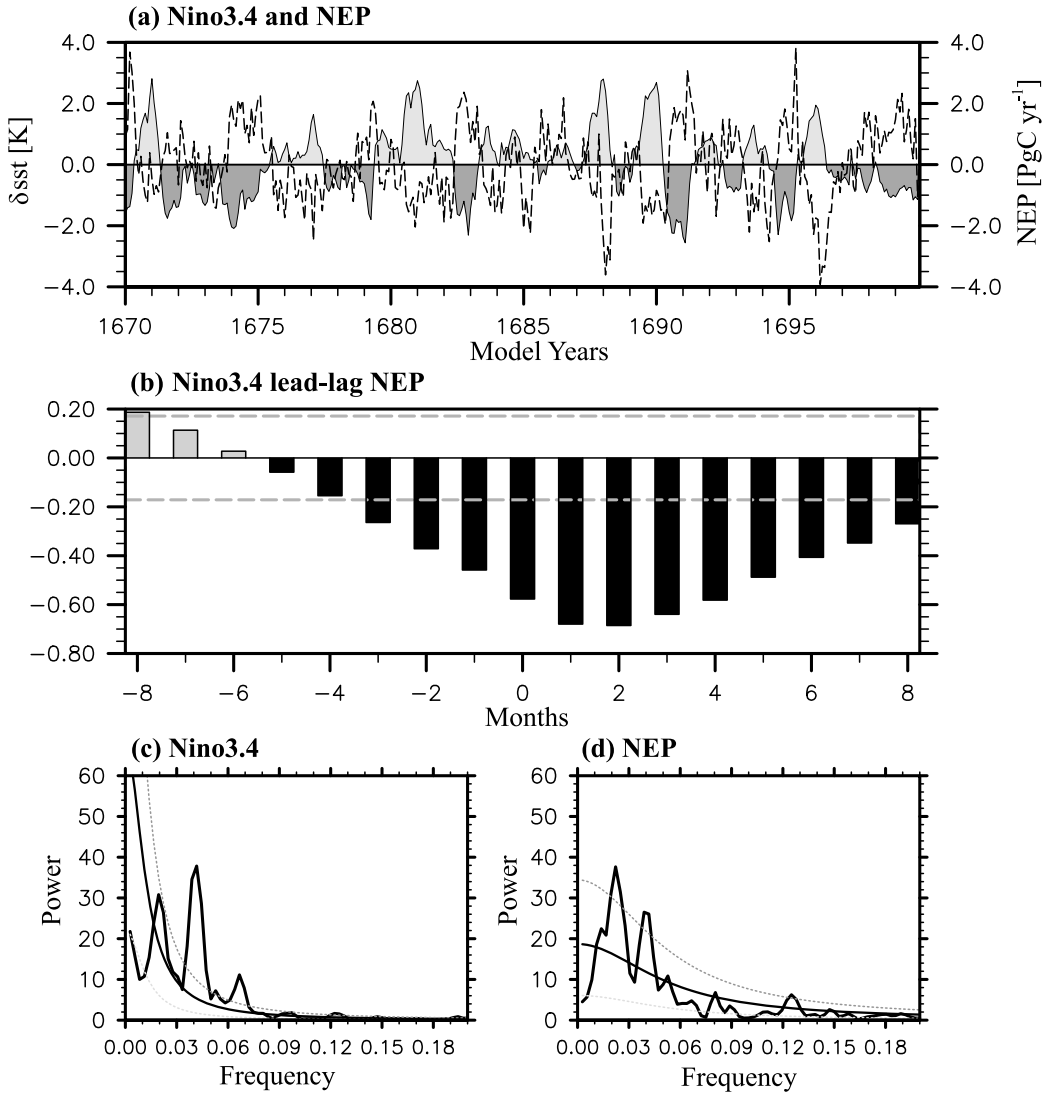

Fig. 7. The relationship between NEP and ENSO, as simulated by ESM FGOALS-s2: (a) time-series of the Niño3.4 SSTA (shaded; units: K) and global total NEP fluctuations (black dashed line; units: PgC yr^{-1}) (seasonal cycle removed); (b) lead-lag correlation between the Niño3.4 index and NEP (gray dashed line denotes the 99% significant level). The positive months represent the Niño3.4 index is prior to the NEP and vice-versa for the negative months. (c) and (d) Power spectral analysis (for the test, the black solid line is the "Markov red noise"; dashed lines represent the 90% and 10% significant levels, respectively).

and CFSR. This variable can truly reflect the performance of the simulation of soil liquid water in ESM FGOALS-s2. Comparing these two figures, we can see that the liquid water volumetric content in the Amazon Basin and northern mid-high latitudes in ESM FGOALS-s2 is about 0.1–0.2 less than in CFSR, whereas it is wetter in Africa near the equator. This result is in accordance with the precipitation bias (Fig. 3a). In East Asia, the soil liquid water volumetric content in ESM FGOALS-s2 is less than in CFSR, which contradicted the precipitation results. Therefore, in order to improve the simulation of soil moisture, being a key point for VEGAS2.0, not only do we need to improve the skill of simulated precipitation in the atmospheric component, but we also need to improve the parameterizations around the water cycle in CLM3.0.

Although the context of this paper delineates the performance of VEGAS2.0 in ESM FGOALS-s2 on the equilibrium state, our goal is to establish a complete ESM concurrently employing an ocean carbon model (Li and Xu, 2012) into the ocean model (LICOM). In the experiment with the full carbon cycle, there is no

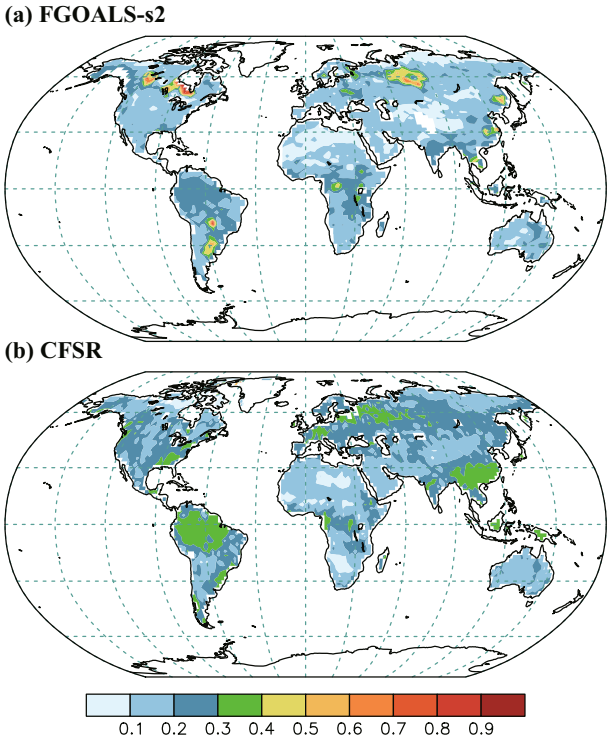

Fig. 8. Distributions of the liquid water volumetric content in land model for (a) liquid water volumetric content in the land component of ESM FGOALS-s2 (model years 1670–99) and (b) CFSR datasets (1979–2000) (Saha et al., 2010). In FGOALS-s2, the lake areas are not well masked.

significant climate drift (Bao et al., 2012). The existing defects will be improved in the next generation ESM version of FGOALS.

6. Concluding remarks

In order to develop an ESM, we successfully incorporated a DGVM (VEGAS2.0) into the PCSM FGOALS-s2. After adopting two spin-up stages, it takes a short time for the coupled model to reach the state of equilibrium, and then we evaluated the performance of equilibrium states with ESM FGOALS-s2 in aspects of climatology, seasonal cycle, and interannual variability. According to the analyses, we uncover some merits as well as shortcomings, summarized as follows.

(1) The simulated global total terrestrial GPP is 124.4 PgC yr^{-1} and NPP/R_h is 50.9 PgC yr^{-1}, which are close to observations. The total terrestrial carbon storage contains 2009.9 PgC, comprising about 628.2 PgC in vegetation and 1381.6 PgC in soil. The spatial distribution of annual-averaged GPP is reasonably simulated, with large values located in the tropics, characterized by rainforests and savannahs.

(2) The seasonal cycle in the tropics is pronounced, especially in NPP and NEP, mainly resulting from the migration of the monsoon rainbelt across the equator from boreal winter to boreal summer. In East Asian monsoon regions, the seasonal cycle caused by air temperature and precipitation changes is also significant.

(3) However, a shortcoming is the simulation of too little vegetation in the northern mid-high latitudes, suppressed by less soil moisture. The less vegetation has a big influence on the distributions of terrestrial carbon storage and seasonal changes (especially LAI). The seasonal cycle of LAI (Fig. 5g) in the northern mid-high latitude is not so significant.

(4) The sensitivity of the terrestrial ecosystem to ENSO is robust. The correlation between them reaches −0.7 as a maximum when the Nino3.4 index precedes NEP for about 1–2 months. Meanwhile, owing to the weak soil memory, the delay of NEP is a little shorter.

The next step is to make some improvements to the shortcomings discussed above, especially in LAI, which is crucial to albedo and evapotranspiration on land. Then, LAI will be returned to the land model in order to establish a more complete and fully coupled ESM.

Acknowledgements. This study was supported by the CAS Strategic Priority Research Program (Grant No. XDA05110303), the "973" programs (Grant Nos. 2012CB417203 and 2010CB950404), the "863" program (Grant No. 2010AA012305), and the National Science Foundation of China (Grant Nos. 41023002 and 40805038).

REFERENCES

Bacastow, R. B., 1976: Modulation of atmospheric carbon dioxide by the Southern Oscillation. *Nature*, **261**, 116–118.

Bao, Q., Y. M. Liu, T. J. Zhou, Z. Z. Wang, G. X. Wu, and P. F. Wang, 2006: The sensitivity of the spectral atmospheric general circulation model of LASG/IAP to the land process. *Chinese J. Atmos. Sci.*, **30**, 1077–1099. (in Chinese)

Bao, Q., G. X. Wu, Y. M. Liu, J. Yang, Z. Z. Wang, and T. J. Zhou, 2010: An introduction to the coupled model FGOALS1.1-s and its performance in East Asia. *Adv. Atmos. Sci.*, **27**, 1131–1142, doi: 10.1007/s00376-010-9177-1.

Bao, Q., and Coauthors, 2012: The flexible global ocean-atmosphere-land system model, spectral version: FGOALS-s2. *Adv. Atmos. Sci.*, **30**(3), 561–576, doi: 10.1007/s00376-012-2113-9.

Beer, C., and Coauthors, 2010: Terrestrial gross carbon dioxide uptake: Global distribution and covariation with climate. *Science*, **329**, 834–838.

Bousquet, P., P. Peylin, P. Ciais, C. L. Quere, P. Friedlingstein, and P. P. Tans, 2000: Regional changes in cabon dioxide fluxes of land and oceans since 1980. *Science*, **290**, 1342–1346.

Brovkin, V., A. Ganopolski, and Y. Svirezhev, 1997: A continuous climate-vegetation classification for use in climate-biosphere studies. *Ecological Modelling*, **101**, 251–261.

Collins, W. D., and Coauthors, 2006: The community climate system model version 3 (CCSM3). *J. Climate*, **19**, 2122–2143.

Cox, P. M., 2001: Description of the "TRIFFID" dynamic global vegetation model. Hadley Center Tech. Note 24, 1–16.

Cox, P. M., R. A. Betts, C. D. Jones, S. A. Spall, and I. J. Totterdell, 2000: Acceleration of global warming due to carbon-cycle feedbacks in a coupled climate model. *Nature*, **408**, 184–187.

Cramer, W., and Coauthors, 1999: Comparing global models of terrestrial net primary productivity (NPP): Overview and key results. *Global Change Biology*, **5**, 1–15.

Denman, K. L., and Coauthors, 2007: Couplings between changes in the climate system and biogeochemistry. *Climate Change 2007: The Physical Science Basis.* Solomon et al., Eds., Cambridge University Press, Cambridge, 499–587.

Dufresne, J. L., P. Friedlingstein, M. Berthelot, L. Bopp, P. Ciais, L. Fairhead, H. Le Treut, and P. Monfray, 2002: On the magnitude of positive feedback between future climate change and the carbon cycle. *Geophys. Res. Lett.*, **29**(10), doi: 10.1029/2001GL013777.

Foley, J. A., I. C. Prentice, N. Ramankutty, S. Levis, D. Pollard, S. Sitch, and A. Haxeltine, 1996: An integrating biosphere model of land surface processes, terrestrial carbon balance, and vegetation dynamics. *Global Biogeochemical Cycles*, **10**, 603–628.

Friedlingstein, P., and Coauthors, 2006: Climate-carbon cycle feedback analysis: Results from the C^4MIP model intercomparison. *J. Climate*, **19**, 3337–3353.

Hagemann, S., 2002: An improved land surface parameter dataset for global and regional climate models. *Max Planck Inst. Meteorol (MPI) Rep.,* **336**, 1–21.

Heimann, M., and M. Reichstein, 2008: Terrestrial ecosystem carbon dynamics and climate feedbacks. *Nature*, **451**, 289–292.

Ji, J. J., 1995: A climate-vegetation interaction model: Simulating physical and biological processes at the surface. *Journal of Biogeography*, **22**, 445–451.

Jones, C. D., M. Collins, P. M. Cox, and S. A. Spall, 2001: The carbon cycle response to ENSO: A coupled climate-carbon cycle and model study. *J. Climate*, **14**, 4113–4129.

Keeling, C. D., and R. Revelle, 1985: Effects of EL Nino/Southern Oscillation on the atmospheric content of carbon dioxide. *Meteoritics*, **20**, 437–450.

Keeling, C. D., R. B. Bacastow, A. E. Bainbridge, C. A. Ekdahl, J. R., P. R. Guenther, and L. S. Waterman, 1976: Atmospheric carbon dioxide variations at Mauna Loa pbservatory, Hawaii. *Tellus*, **28**, 538–551.

Levis, S., G. B. Bonan, M. Vertenstein, and K. W. Oleson, 2004: The community land model's dynamic global vegetation model (CLM-DGVM): Technical description and user's guide. NCAR Tech. Note, NCAR/TN-459+IA, 64pp.

Li, Y. C., and Y. F. Xu, 2012: Uptake and storage of anthropogenic CO_2 in the Pacific Ocean estimated using two modeling approaches. *Adv. Atmos. Sci.*, **29**, 795–809, doi: 10.1007/s00376-012-1170-4.

Mitchell, T. D., and P. D. Jones, 2005: An improved method of constructing a database of monthly climate observations and associated high-resolution grids. *Inter. J. Climatol.*, **25**, 693–712.

Myneni, R. B., R. R. Nemani, and S. W. Running, 1997. Algorithm for the estimation of global land cover, LAI and FPAR based on radiative transfer models. *IEEE Trans. Geosc. Remote Sens.*, **35**, 1380–1393.

Oleson, K. W., and Coauthors, 2004: Technical Description of the Community Land Model (CLM). NCAR/TN-461+STR, 174pp.

Qian, H. F., R. Joseph, and N. Zeng, 2008: Response of the terrestrial carbon cycle to the El Nino-Southern Oscillation. *Tellus*, **60B**, 537–550.

Qian, H. F., R. Joseph, and N. Zeng, 2009: Enhanced terrestrial carbon uptake in the northern high latitudes in the 21st century from the coupled carbon cycle climate model intercomparison project model projections. *Global Change Biology*, **16**, 641–656.

Saha, S., and Coauthors, 2010: The NCEP climate forecast system reanalysis. *Bull. Amer. Meteor. Soc.*, **91**, 1015–1057.

Taylor, K. E., R. J. Stouffer, and G. A. Meehl, 2009: A summary of the CMIP5 experiment design. [Available online at http://cmip-pcmdi.llnl.gov/cmip5/docs/Taylor_CMIP5_design.pdf.]

Zeng, N., 2003: Glacial-interglacial atmospheric CO_2 change — The glacial burial hypothesis. *Adv. Atmos. Sci.*, **20**, 677–693.

Zeng, N., H. F. Qian, E. Munoz, and R. Iacono, 2004: How strong is carbon cycle-climate feedback under global warming? *Geophys. Res. Lett.*, **31**, L20203, doi: 10.1029/2004GL020904.

Zeng, N., A. Mariotti, and P. Wetzel, 2005: Terrestrial mechanisms of interannual CO_2 variability. *Global Biogeochemical Cycles*, **19**, GB1016, doi: 10.1029/2004GB002273.

Zhang, X. H., G. Y. Shi, H. Liu, and Y. Q. Yu, 2000: *IAP Global Ocean-Atmosphere-Land System Model.* Science Press, Beijing, 252pp. (in Chinese)